J Mater Sci: Mater Med (2010) 21:1297–1309
DOI 10.1007/s10856-009-3942-7

In vitro cellular adhesion and antimicrobial property of SiO_2–MgO–Al_2O_3–K_2O–B_2O_3–F glass ceramic

Sushma Kalmodia · Atiar Rahaman Molla · Bikramjit Basu

Received: 19 August 2009 / Accepted: 10 November 2009 / Published online: 20 November 2009
© Springer Science+Business Media, LLC 2009

Abstract The aim of the present study was to examine the cellular functionality and antimicrobial properties of SiO_2–MgO–Al_2O_3–K_2O–B_2O_3–F glass ceramics (GC) containing fluorophlogopite as major crystalline phase. The cellular morphology and cell adhesion study using human osteoblast-like Saos-2 cells and mouse fibroblast L929 cells reveals good in vitro cytocompatibility of GC. The potential use of the GC for biomedical application was also assessed by in vitro synthesis of the alkaline phosphatase (ALP) activity of Saos-2 cells. It is proposed that B_2O_3 actively enhances the cell adhesion and supports osteoconduction process, whereas, fluorine component significantly influences cell viability. The Saos-2 and L929 cells on GC shows extensive multidirectional network of actin cytoskeleton. The in vitro results of this study illustrate how small variation in fluorine and boron in base glass composition influences significantly the biocompatibility and antimicrobial bactericidal property, as evaluated using a range of biochemical assays. Importantly, it shows that the cell viability and osteoconduction can be promoted in glass ceramics with lower fluorine content. The underlying reasons for difference in biological properties are analyzed and reported. It is suggested that oriented crystalline morphology in the lowest fluorine containing glass ceramic enhanced cellular spreading. Overall, the in vitro cell adhesion, cell flattening, cytocompatibility and antimicrobial study of the three different compositions of glass ceramic clearly reveals that microstructure and base glass composition play an important role in enhancing the cellular functionality and antimicrobial property.

S. Kalmodia · B. Basu (✉)
Laboratory for Biomaterials, Department of Materials and Metallurgical Engineering, Indian Institute of Technology Kanpur, Kanpur 208016, India
e-mail: bikram@iitk.ac.in

A. R. Molla
Glass Division, Central Glass and Ceramic Research Institute, Council of Scientific and Industrial Research, Kolkata, WB, India

1 Introduction

In last few decades, glass ceramics are being developed for repair and replacement of damaged tissue [1, 2]. In the development of GC, the base glass is heat treated in a desired temperature—time window and crystals of various morphology and amount can form. Because of the presence of crystalline phase, glass ceramics have more favorable mechanical and biological properties than pure glass. Numerous clinical trials have shown intergrowth between glass–ceramics and human bone [3]. The important clinical applications of glass ceramic are related to the repair of skeletal system, which is composed of bone, joints and teeth. In order to achieve better combination of physical and biological properties, a number of researchers attempted to tailor composition and properties in various GC systems, which include SiO_2–CaO–Na_2O–P_2O_5, SiO–$_2$CaO–MgO–P_2O_5–F, SiO_2–Al_2O_3–MgO–CaO–Na_2O–K_2O–P_2O_5–F.

Hench's study first demonstrates that bioactive glasses (45S5 series) and bioactive glass–ceramics belong to two different classes of bioactive implants, i.e. Class A and Class B, respectively, due to large differences in the rate of bone bonding [4]. Machinable bioactive glass–ceramics containing microcrystalline phases of mica and apatite can be considered as class B bioactive implants [5]. Bioactivity is a property displayed by ceramics such as bioglass, hydroxyapatite and glass–ceramic A–W and is characterized by chemical integration of synthetic materials with

living tissue [6]. For example, a boron based bioactive GC can exhibit more rapid hydroxyapatite layer formation than bioactive 45S5 series glasses. Additionally, it also supports the growth and differentiation of mesenchymal stem cells [7–10]. A core mechanism of bioactivity is the biomineralization of calcium phosphate nano-crystals on ceramics with specific compositions and structures [11]. The bioactive GC containing boron and fluorine help in extracellular secretions of ECM components, such as proteoglycans, protein. This assists in mineralization by increased Ca/P ratio and provides anti-microbial properties, which combinedly make them a potential material for the orthopedic implant [12].

GC is also a good candidate material for the dental implant, and the primary requirement for successful use of GC for dental applications is the anchoring and attachment with bone tissue. Therefore, it is necessary to use different kinds of connective tissue cell line like, L929 fibroblast and osteoblast like cell Saos-2 and such cells must be interfaced with the implant material. Harrison et al. studied the differentiation of embryonic stem cell (ES) on hydroxyfluorapatite [11]. It was also reported that fluroapatite mullite coating on biomaterial surface has capacity of osteoblast differentiation [13]. In vitro study of cell viability/proliferation on the surface of a biomaterial is an indicator of biocompatibility and can be evaluated by MTT assay and cell adhesion test [11, 14].

Liu and co-workers studied behavior of mica/apatite glass–ceramics in simulated body fluid (SBF) solution and found good bioactivity [15]. In vitro bioactivity of wollastonite glass–ceramic materials were carried out by Alemany et al. and the formation of Hydroxyapatite (HA) layer on the material surface was observed after immersion in SBF [16]. The HA forming ability of $CaMgSi_2O_6$–$Ca_5(PO4)_3F$–$CaAl_2SiO_6$ glass ceramics has also been reported by Salama and co-workers [17]. Verne et al. found that antimicrobial effect of Ag based bioglass is due to leaching of Ag from the glass matrix, change in pH and ionic strength [3]. Brook et al. studied the in vitro effect of leached ions on viability of cells and conclude that fluoride ions exhibited mild toxicity effect on the osteoblast and fibroblast cells [18]. Moreover, leached ions significantly affect the microbial growth and adhesion on sample surface. Soljanto et al concluded that bacterial growth inhibition depends on the concentration and size of the material, such as fluorapatite and glass beads etc. in the culture medium [19]. Armstrong et al. concluded that an antibiotic actinobolin and fluorine ion mutually prevents the dental caries and periodontal disease and increased mineralization on sample surface. As a part of our ongoing research in the area of glass ceramics, the present work reports the osteoconduction [20], cytotoxicity and antimicrobial property of the K_2O–B_2O_3–Al_2O_3–SiO_2–MgO–F glass ceramics, fabricated by heat treating three different base glass compositions under identical conditions. Our previous results of in vitro dissolution study show that bioactive GC, leached F^-, K^+, Mg^{2+}, Ca^{+2} ions and form the hydroxyapatite layer [21]. In the above background, the objective of the present investigation was to elucidate the effect of microstructure and compositions on the biological properties such as cytocompatibility and antimicrobial activity of GC. In addition to this, cellular behavior such as cell adhesions, cell spreading and proliferation are also evaluated.

2 Experimental procedure

2.1 Materials

In continuation of our earlier work [21], three compositions with varying fluorine and B_2O_3 content in the K_2O–MgO–Al_2O_3–B_2O_3–SiO_2–F have been studied in the present work (Table 1). The starting materials were highly pure optical grade Quartz (SiO_2), Al_2O_3, MgO, K_2CO_3, H_3BO_3, Na_2CO_3 and MgF_2. Glass batches were well mixed and thereafter melted in a platinum crucible at 1550°C for 2 h using electrical furnace. The glass melts were cast into a cast iron mould to form plates, and then annealed for 2 h in the temperature range of 600–650°C. The annealing conditions were selected in order to avoid nucleation at this stage. The compositions of the base glasses were analyzed by ICP AES (Inductive coupled plasma-atomic emission spectroscopy: spectroflame modula FTM08, Germany). XRD study indicated the amorphous nature of as-prepared glasses. The heat treatment of all the three base glasses has been carried out at 1040°C for 12 h. XRD study of the glass ceramics revealed predominant presence of fluorophlogapite phase in all the glass ceramics. Detailed analysis of the FT-IR data confirmed the presence of various Si–O–Si, Si–O and B–O stretching bonds with the characteristic absorption peaks at 1022, 697 and 1422 cm^{-1}, respectively. In addition, Si–O–Si bonds cause FT-IR peak as 465–509 cm^{-1}.

Table 1 Compositions of base glass (in wt%) used in the present work

Starting materials	Precursor constituent	M1	M2	M3
Quartz powder	SiO_2	47.98	48.94	42.57
White tabular alumina	Al_2O_3	17.62	16.29	17.81
MgO powder	MgO	19.36	17.45	18.80
K_2CO_3	K_2O	8.25	7.15	7.81
Boric acid (H_3BO_3)	B_2O_3	5.17	5.25	10.02
NH_4F/MgF_2	F^-	1.08	3.85	2.53

2.2 Cell culture experiments

In this study, Mouse fibroblast (L929) and Human osteoblast like cells (Saos-2) cell lines were used for cell-culture experiments. Before seeding the cells on GC surfaces, the cells were revived in tissue culture graded culture plate. The cryo-vial was rapidly thawed and cells were cultured in Dulbecco's modified Eagles medium (DMEM, including 300 mg/l L-glutamine, 2 g/l sodium bicarbonate) supplemented with 10% heat-inactivated FBS, (Sigma-Aldrich), 1% of antibiotic antifungal cocktail (10,000 IU penicillin 10 mg streptomycin and 25 μg amphotericin B/ml) at 37°C temperature in a 5% CO_2 humidified atmosphere. The sub-confluent monolayer (approximately 5×10^5/ml, in 35 mm culture plate) was trypsinized using 0.5% trypsin and 0.2% EDTA solution (Sigma-Aldrich). The above protocol is followed for subculture.

As part of cellular adhesion tests, L929 and Saos-2 cells were maintained in DMEM culture medium supplemented with 10% heat-inactivated FBS, 1% of antibiotic antifungal cocktail at 37°C in a 5% CO_2 humidified atmosphere. These glass ceramic samples of $4 \times 4 \times 4 \times$ mm dimension and glass cover slip of 12 mm diameter, coated with 0.2% purified gelatin, were used for cell adhesion experiments. The samples were ultrasonically cleaned, sterilized in autoclave (121°C, 15 lb pressure) and placed under ultraviolet light in a hood for 30 min. Following this, the sterilized samples were soaked in 70% ethanol. The surface was washed twice with warm phosphate buffer (PBS, pH 7.4). Subsequently, the cells were seeded on the samples at a density of 3×10^5/ml in 24 well culture plates and culture under standard cell culture condition, 5% CO_2, 37°C and 95% humidity. The cell density was measured by Haemocytometer (improved NEUBAUER, DEEPTH 0.1 mm). After 48 h of fibroblast (L929) and 72 h of osteoblast like cell (Saos-2) cells culture, the material surface was washed with PBS and then fixed with 2% glutaraldehyde in PBS for 30 min. The cells, adhered on the materials surface, were dehydrated using a series of ethanol solutions (30, 50, 70, 95 & 100%) for 10 min twice at each dilution level and then further dried using hexamethyldisilazane (HMDS, Sigma) for 10 min. The dried samples were sputter coated with gold and detailed analyses of cell adhesion behavior were carried out using SEM (Philips, Quanta).

2.3 MTT assay

The modified colorimetric method of Mosmann [22] has been used to confirm the survival and proliferation of mammalian cells in contact with a material. MTT (3(4,5-dimethylthiazol-2-yl)—2,5-diphenyl tetrazolium bromide)) is a rapid colorimetric method and is widely adopted for quantification of cytotoxicity and cell proliferation. The cell proliferation and cytocompatibility were investigated on three different GC compositions, (M1, M2 and M3, all heat treated at 1040°C, 12 h), HAp (sintered at 1200°C, 2 h) and glass cover slip. The samples were seeded at approximate cell density of 3×10^4/ml by L929 cells. The MTT assay was performed on days 2, 4, and 6 days after the cell are seeded on the sample. After the incubation, the sample was washed twice with PBS and reconstitute MTT (5 mg/ml MTT in DMEM culture medium without Phenol red and serum) with 10 μl/100 μl of DMEM culture medium was added. Subsequently, the culture plate was incubated for 4–6 h in CO_2 incubator at 37°C. In the meantime, culture plate was viewed in the phase contrast microscope (Nikon- Eclipse 80i, Japan) to check the formation of purple formazan crystal. Subsequently, the medium and MTT solution was aspirated and samples were washed with PBS. The insoluble formazan crystal was dissolved by adding 200 μl of Dimethylsulphoxside (DMSO) and culture plate was rocked for 15 min. The samples were removed from wells and optical density of the solutions were measured at 630 nm using ELISA Automated Microplate Reader (Bio-Tek, model ELx800). The quantification of the Cell proliferation/viability in terms of metabolically active cells was calculated using the formula,

$$\% \text{ Viability} = \text{Mean Absorbance of Sample} / \text{Mean Absorbance of Control} \times 100$$

2.4 Osteoblast phenotypic marker, ALP assay

The functionality of proliferated Saos-2 cells was studied by examining the production of alkaline phosphatase. The osteoblast like cells Saos-2 were culture on the GC and glass cover slip for 1 week. Once the sub-confluent stage is attained, the culture medium was changed by the differentiating medium, which includes DMEM supplemented with 10% FBS, 1% Penn/Strep, cholecalciferol (vitamin D_3) (10^{-8} m final concentration), ascorbic acid (50 μg/ml final) and beta-glycerol phosphate (8 mmol final). After 1 week of culture, the culture medium was removed and adherent cells were washed twice with PBS without phosphate. Subsequently, the Alkaline lysis buffer (10 mM Tris-HCl, 2 mM $MgCl_2$, 0.1% Triton X-100, pH 10) (100 μl/well) was added and the samples were scrapped and then frozen at −20°C for 30 min. Subsequently, the freeze and thaw cycle was repeated two times and cell lysate was used for the ALP activity. The ALP activity was measured colorimetrical, while adding 25 μl of an aqueous solution of *p*-nitrophenyl phosphate (PNPP; pH—10.5) into the cell lyset. Then, the entire system was incubated at 37°C for 20 min. The ALP enzyme expressed by the cells hydrolyzed the substrate to *p*-nitrophenol and an inorganic

phosphate. The reaction was stopped by adding 50 mM NaOH and the optical density was measured at 405 nm.

2.5 Bacterial adhesion and antimicrobial properties

The bacterial strain of *Staphylococcus epidermidis* (ATCC NO #35984) and *Escherichia coli*, (ATCC#25922) were used to assess the in vitro antimicrobial properties of the glass ceramic samples. The above mentioned bacterial strains were procured in the freeze dried condition from the American Type Culture Collection (ATCC). Prior to seeding on the sample surface, bacteria were inoculated in a Luria–Bertani broth, supplemented with yeast and beef extract, and culture was incubated overnight at 37°C. In order to obtain pure culture, the streaking on agar plate was done with suspension culture to isolate the single colony. The single colony was picked from the agar plate and inoculates in the freshly prepared Luria–Bertani broth. The culture was incubated over night for growth. The pure suspension culture of bacterial density of 1×10^7 CFU/ml/well was used for seeding on the samples.

The seeded samples were incubated and bacteria allowed adhering up to 4 h. Subsequent to the incubation period, the surface was rinsed with PBS and then soaked in primary fixative of 3% glutaraldehyde, 0.1 M sodium cacodylate, and 0.1 M sucrose for 45 min. The surface was washed twice with PBS buffer. The cells were dehydrated by replacing the buffer with ethanol series 30, 50, 70, 95 and 100% for 10 min each and then, further dried by 100% hexamethyldisilazane (HMDS) for 10 min. The dried samples were sputter coated with gold and examined under SEM. Turbidometric analysis was also performed after 4 h of incubation. Followed by washing of sample with PBS, each sample was placed in 3 ml volume of PBS solution and vortexed sufficiently to remove the adherent bacterial cell from the sample surface. Subsequently, sample was removed from PBS and optical density (OD) of PBS suspensions was measured at 660 nm wavelength using UV–VIS spectrophotometer (Thermo Scientific UV-10, UK). The bacterial adhesion on the sample surface was expressed in terms of optical density (OD).

2.6 Statistical analysis

The in vitro tests described above were run in triplicate. The commercial SPSS-13 software was used for statistical analysis. The statistical analysis was carried out by analysis of variance (ANOVA). The post–hoc comparisons of the means of independent groups were performed using Tukey test at statistically significant value ($P < 0.05$). The error bars associated with each data point represent standard error (n = No. of replicates, $n = 6$ for cell adhesion, $n = 6$ for MTT assay, $n = 6$ for ALP assay and $n = 6$ for antimicrobial test).

3 Results

It is imperative to study the microstructure of the investigated glass ceramic surfaces before the biocompatibility study. Therefore, SEM analysis was carried out to study crystal shapes, size and size distribution in various heat-treated glass–ceramic samples of varying composition. In Fig. 1a, SEM image of M1 glass–ceramic, crystallized at 1040°C for 12 h is provided. The presence of large rod like crystals, aligned in specific directions can be clearly observed in Fig. 1a. In Fig. 1b, SEM images of M2 glass ceramics, crystallized for 12 h at a temperature of 1040°C, is provided. SEM analysis reveals crystals with sizes in the range of 5–10 μm. In Fig. 1c, SEM image illustrates the presence of dense arrangement of crystals in M3 glass ceramic and it also reveals the presence of hexagonal shaped and rod likes crystals. The average crystal size of hexagonal shaped crystals was observed to be around 2–5 μm. Rod like crystals of 1–4 μm length were also seen. More detailed information on processing—microstructure physical properties relationship of the investigated glass ceramics can be found in our recent paper [21].

3.1 Cellular adhesion behavior

Figures 2 and 3 present the scanning electron microscopic evidences of the cellular adhesion of L929 and Saos-2 cells on control M1, M2 and M3 GC after 48 h and 72 h of culture, respectively. It can be noted that L929 cells are used in compliance with the biocompatibility testing, as outlined in ISO 10993-5 guideline for in vitro test. Moreover, fibroblast cell (L929) is least specialized and easily proliferate on substrates. Therefore, the optimized culture time was 48 h [23]. While L929 are cells of connective tissues and least specialized, osteoblast like cells is (Saos-2) differentiated and specialized cell line. The optimized cell culture time for Saos-2 was 72 h in order to assess whether investigated GC can support the osteoconduction property. The use of two different cell lines was important as the presently investigated GC are being developed as candidate material for the biomedical applications. From Figs. 2 and 3, it is clear that L929 mouse fibroblast and osteoblast like cell Saos-2 shows difference in morphology and adhesion behavior on GC samples. Following this, some interesting observations can be made about cell-adhesion behavior on M1, M2 and M3 GC samples with both the cell lines. Figures 2 and 3 clearly reveals the cell proliferation (a coordinated process of growth and division) and cell–cell contacts on M1, M2 and

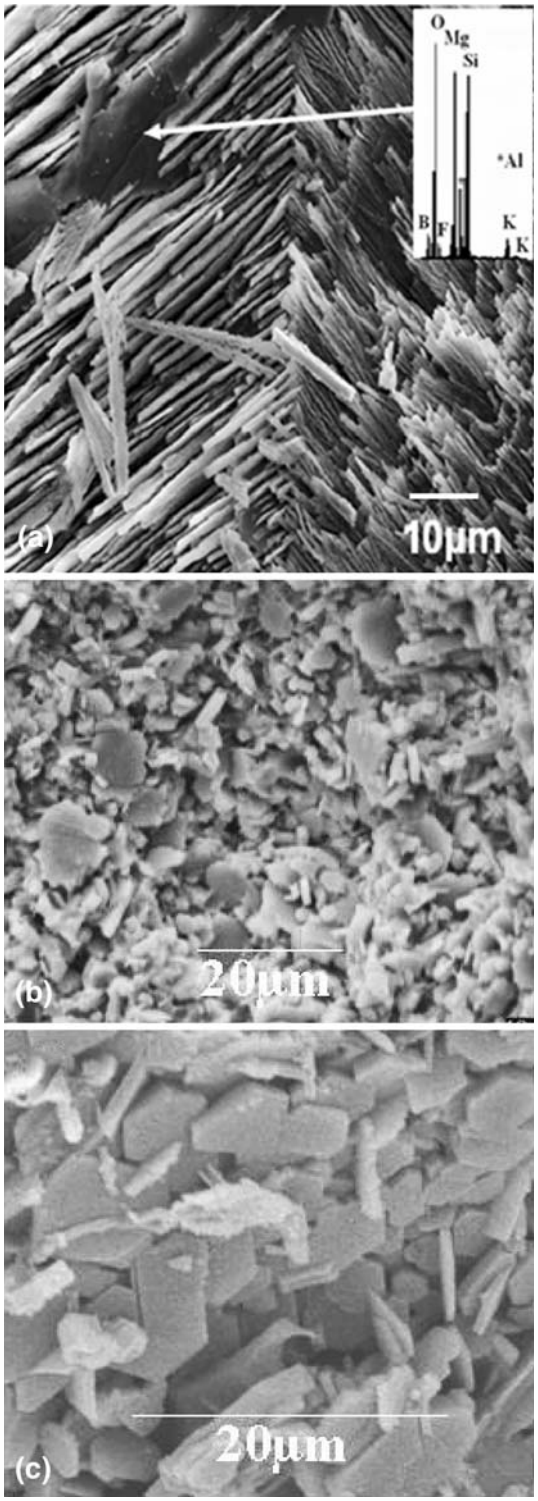

Fig. 1 SEM micrographs of the polished surface of three investigated glass–ceramic crystallized for 12 h at a temperature of 1040°C. **a** M1, **b** M2 and **c** M3

M3 GC samples. It has been observed that cell proliferation and cell-to-cell contacts are more in M2 and M3 GC sample as compared to M1 sample. However, cell flattening with very little actin cytoskeleton protrusions were noticed on the M1 (Figs. 2a, 3a). In contrast, cells were fully spread on M2 and M3 samples with multiple lamellae extended in all the directions (Figs. 2, 3). Other noticeable difference was that L929 showed significantly higher filopodium and lamellipodium extension.

3.2 Cellular viability

It is well known that MTT reagent directly reacts with the mitochondria (Mitochondrial dehydrogenase enzyme) of metabolically active cells. Figure 4 plots the MTT assay results, obtained using mouse fibroblast cells (L929) on three GC samples. The results are presented as % viability of cells with reference to control disc. For the M1 sample, the numbers of metabolically active cells are statistically higher than that of the control (see Fig. 4). The cytotoxicity of M1, M2 and M3 GC was measured on 2nd, 4th and 6th days of culture. Among the test samples, M1 and M2 GC showed significant difference with M3. The M1 samples exhibited a maximum of 161.78% cell viability after 2 days of culture. The percent viability was reduced significantly on the 4th and 6th days. Also, significant difference was noticed in the cytocompatibility results as a function of culture duration between all the samples at $P < 0.05$. The rank of cytotoxicity is M1 < M2 < M3. In conclusion, MTT results clearly shows that M1 sample is the best cytocompatible material among all the investigated glass ceramics.

3.3 Osteoblastic phenotypic marker (ALP)

Alkaline phosphatase, an ectoenzyme produced by osteoblast is involved in the degradation of inorganic pyrophosphate for mineralization to support the differentiation of cells. It needs to be mentioned here that Saos-2 cell line are already in differentiated stage and the purpose of carrying out ALP assay is to assess whether further differentiation of Saos-2 cell line is supported by investigated glass ceramics. It can be further said that most of the Saos-2 cells of same passaging stage, having same differentiated stage, are seeded on all the three glass ceramic surfaces. Therefore, difference in ALP expression should primarily be attributed to difference in substrate composition or difference in ability of GC to promote further differentiation. The characteristics ALP activity of Saos-2 on control and the GC sample was assessed after 7 days of culture. M1 sample showed highest ALP activity and significant difference was noticed between the M2 and M3 sample with respect to control (see Fig. 5). The ALP activity decreased significantly in M2 and M3 sample, when compared to control sample. Based on the statistical significance analysis at $P < 0.05$, ALP activity on different GC can be ranked as M1 > M2 > M3.

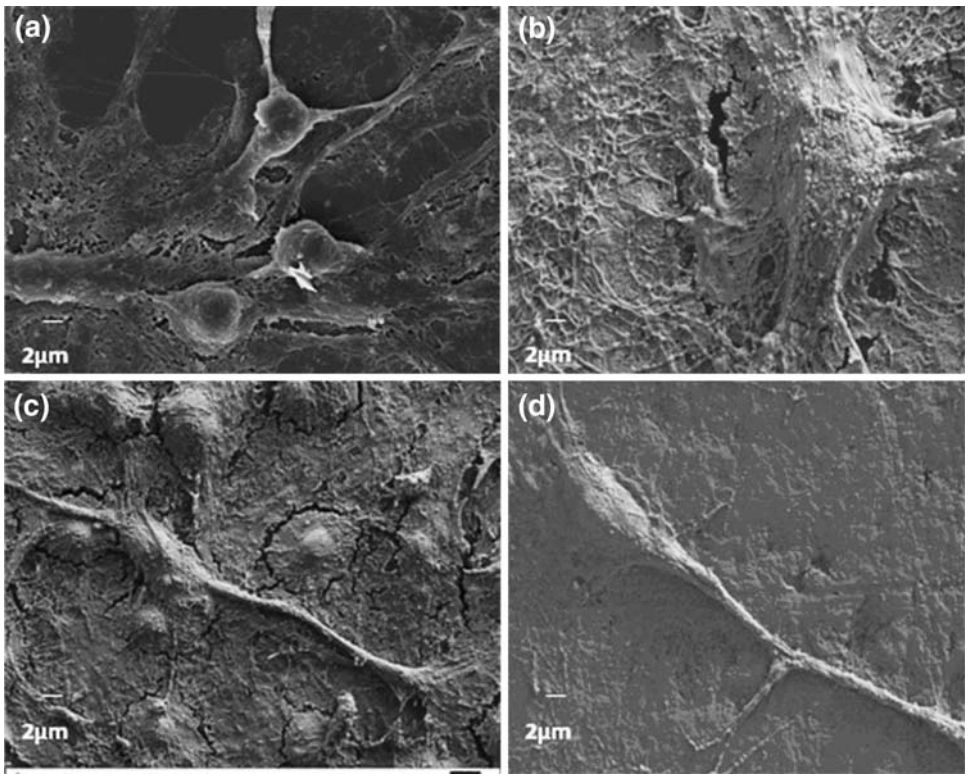

Fig. 2 SEM micrographs of adhesion and spreading behavior Saos-2 Osteosarcoma cell on **a** Control, **b** M1, **c** M2 and **d** M3 GC samples. The Dorsal ruffles, microspikes and filipodium are formed on the M1 surface, whereas M2 and M3 show Lamellipodia. The control material shows a normal osteoblast flattened morphology without any actin filament extension

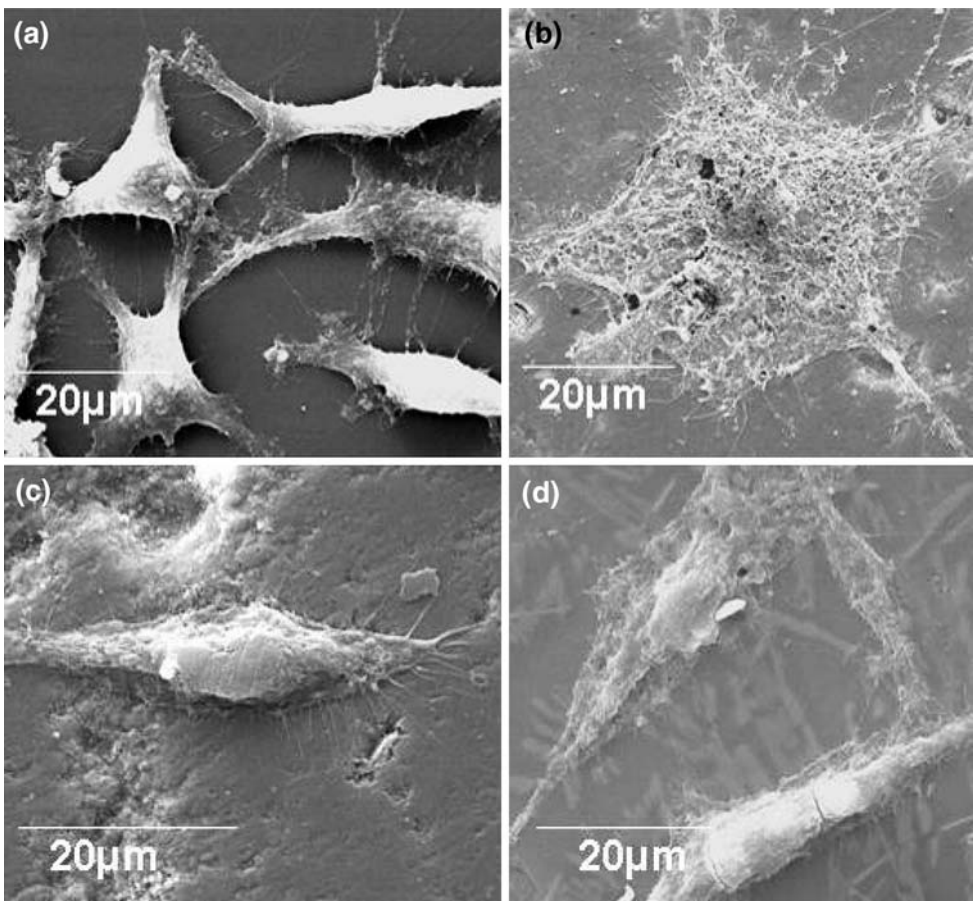

Fig. 3 Scanning electron micrographs of L929 Mouse fibroblast cells grown on on **a** Control, **b** M1, **c** M2 and **d** M3 glass ceramic samples. The Microspikes and filipodium are formed on the M1 surface, whereas M2 and M3 show Lamellipodia

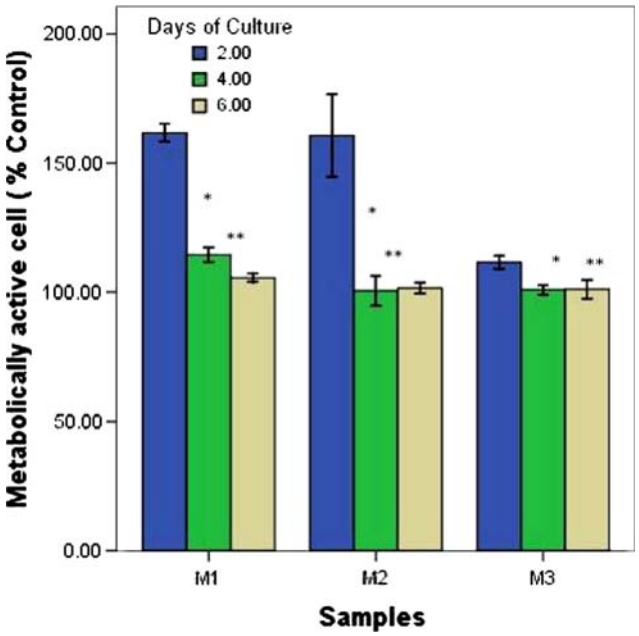

Fig. 4 The cell viability evaluation of metabolically active L929 fibroblast cell, after 2, 4 and 6 days of culture on M1, M2 and M3 samples. The cells were seeded initially at a density of 3×10^5 cells/ml. * Represent significant difference at among the samples $P < 0.05$ and error bars correspond to ± 1.00 SE. The M1 shows significant difference with M2 and M3. ** Represent significant difference at among the days of culture $P < 0.5$. The 6 days of culture shows significant difference with 2 and 4 days of culture

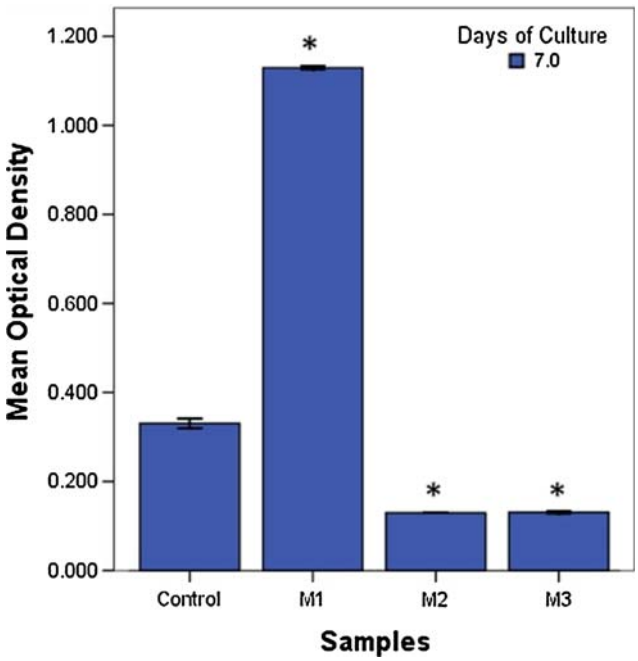

Fig. 5 Alkaline phosphatase (ALP) activity of the Saos2 cells on M1, M2 and M3 GC and control (Gelatin coated glass cover slip) after 7 days of culture in osteogenic medium. The M1, M2 and M3 show significant difference with respect to control disc. The cells were seeded initially at a density of 3×10^5 cell/ml. * Represent significant difference at $P < 0.05$ among sample sand error bars correspond to ± 1.00 SE

3.4 Antimicrobial property

Figures 6 and 7 presents representative SEM images, revealing bacteria adhesion and antimicrobial properties against Gram-positive *S. epidermidis and* Gram- negative *E. coli* bacteria after 4 h of incubation on the test samples in vitro. On the basis of the statistical analysis of the optical density results (Figs. 8, 9) as well as SEM observation M1 and M2 GC shows the bacteriostatic effect (adherence, but not killing of bacteria) against Gram negative as well Gram positive bacteria (Figs. 6b–e, 7b–e); whereas M3 samples show bactericidal effect (killing of bacterial cells) compared to other two samples (Fig. 6d, 7d). SEM images also reveal the lack of much difference between the samples in there antimicrobial properties of *E. coli* and *S. epidermidis*, but such images however show noticeable difference with respect to control sample. It was clear that there was no colonization and biofilm formation of *S. epidemidis* and *E. coli* on the surface of GC samples. After 4 h incubation of *S. epidemidis,* the number of bacterial colony forming unit adhered on control material was approximately 1×10^7 CFU/ml. In contrast to control material, the number of CFU adhere on M1, M2 and M3 GC were approximately, 1.2×10^6 CFU/ml, 1.38×10^6 CFU/ml and 0.96×10^6 CFU/ml, respectively. The M3 sample showed highest antimicrobial activity with approximately 16% of CFU/ml was observed as compared to the control material.

4 Discussion

It is recognized that glass ceramics of suitable composition are one among the desired class of biomaterials for biomedical application due to their good machinability, bioactivity and favorable mechanical properties. The biocompatibility property however is not extensively studied for various glass ceramics. It has been widely reported that glass ceramics demonstrating favorable properties can be developed with variation in chemical composition and crystal morphology [24]. The present study focused on the influence of glass ceramic composition and microstructure on the biocompatibility of M1, M2 and M3 glass ceramic. The boron and fluoride derivatives are well known for their effects on the biological properties, as they help in extracellular secretion of ECM component and antimicrobial activity, respectively. The characteristics of microstructure such as crystal orientation, crystal content, size and morphology also influence the biological responses.

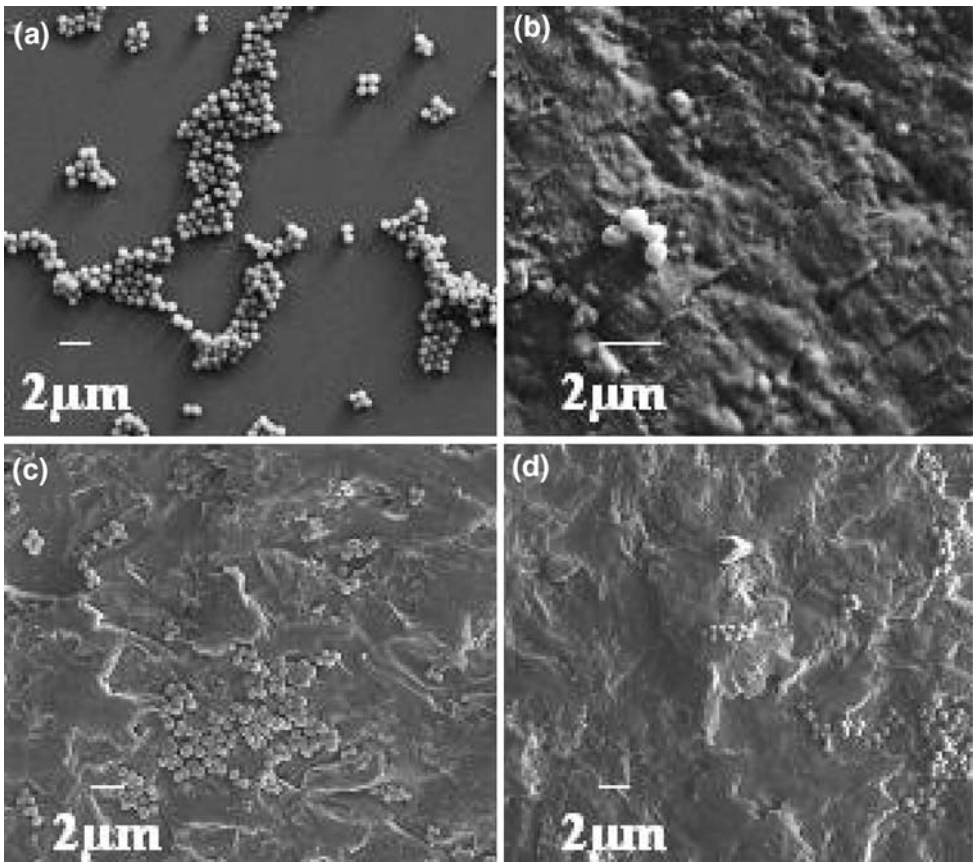

Fig. 6 SEM Electron Micrograph of the *Staphylococcus epidermidis* bacteria colony after 4 h of incubation on **a** Control, **b** M1, **c** M2 and **d** M3 glass ceramic samples

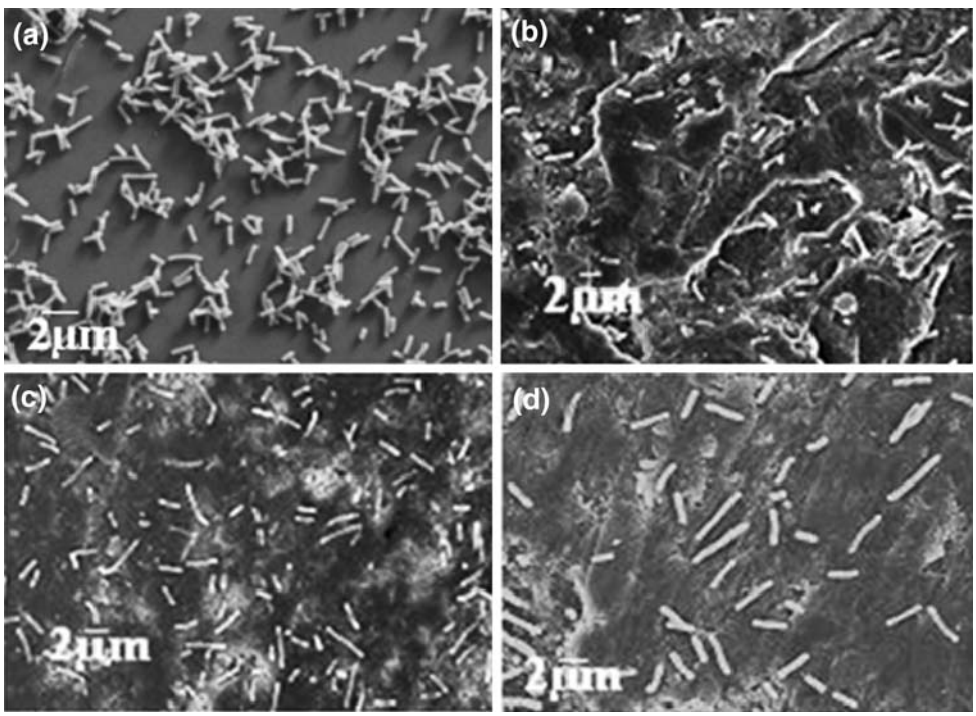

Fig. 7 SEM Electron Micrograph of the *Escherichia coli* bacteria after 4 h of incubation on **a** Control, **b** M1, **c** M2 and **d** M3 glass ceramic samples

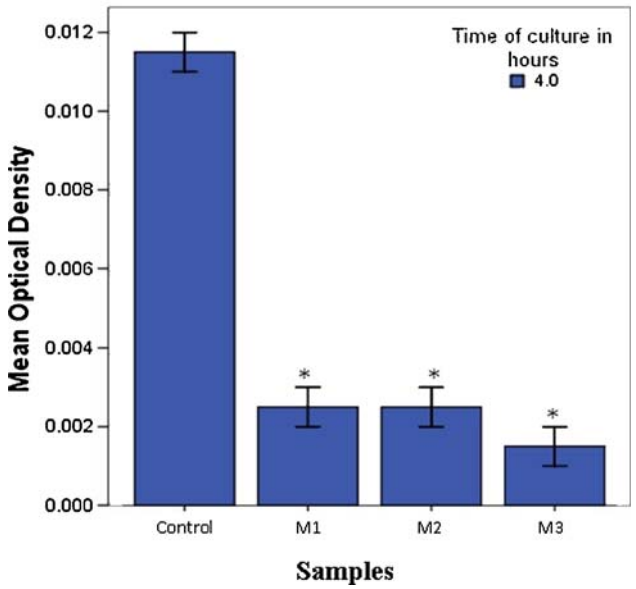

Fig. 8 Mean OD value after 4 h incubation of *Staphyloccous epidermidis* bacterial on control, M1, M2 and M3 GC. The Initial bacterial inoculum contains 1×10^7 CFU/ml. * Represent significant difference at among samples $P < 0.05$ with respect to control disc and Error bars correspond to ±1.00 SE

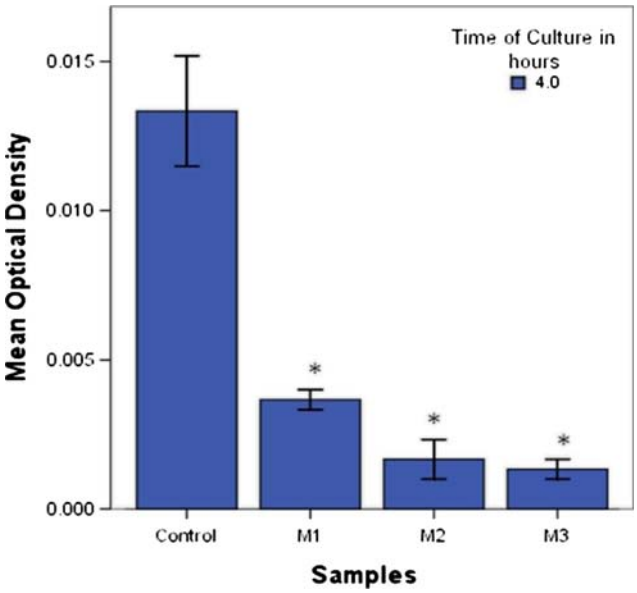

Fig. 9 Mean OD value after 4 h incubation of *Escherichia coli* bacterial on control, M1, M2 and M3 GC. The Initial bacterial inoculum contains 1×10^7 CFU/ml. * Represent significant difference at $P < 0.05$ with respect to control disc and Error bars correspond to ±1.00 SE

4.1 Influence of microstructure and composition on cytocompatibility

In order to discuss the influence of base glass composition and microstructure on cytocompatibility property, it is instructive to first summarize the salient features of microstructure and glass composition. Figure 1a illustrates that the SEM micrograph of M1 sample, which reveals anisotropic rod/plate like crystals within crystal domain. In contrast, crystals are homogeneously distributed and densely packed in both M2 and M3 glass ceramics. While a few hexagonal shaped crystals are observed in M2 GC sample (Fig. 1b), such crystals with sizes of 4–5 μm are predominant in M3 GC sample (Fig. 1c). As far as the microstructural influence on cellular adhesion is concerned, it can be said that the oriented crystalline morphology possibly enhanced the cell adhesion as well as cell spreading. This can explain better cellular viability of M1 glass ceramic in comparison to M2 or M3 glass ceramic. It is reported in literature that scaffolds with polymeric nanofibers having oriented morphology supports enhanced cellular functionality (viability, migration etc.) compared to scaffolds with randomly oriented nanaofibers [25]. Therefore, orientation of microstructural features appears to influence cell adhesion property. The present work therefore reconfirms that oriented crystal morphology in glass ceramics also supports cellular viability as well as promotes osteoblast differentiation.

As far as the compositional aspect is concerned, the composition of base glass (not starting powder mix) was measured using ICP-AES and the results are presented in Table 1. It is clear that the base glass has SiO_2 as major constituent. As far as amount of B_2O_3 is concerned, M3 has little less than two times B_2O_3 than that of M1 and M2, which have almost similar B_2O_3 content. With respect to fluoride concentration, M1 has lowest and M2 has highest amount, while M3 has intermediate content. From the present experimental results, GC with lowest F^- content has the best cytocompatibility property.

As far as the cell-material interaction is concerned, initial attachment of cell is mediated by the integrins, a transmembrane protein which connect the extracellular matrix (ECM) to the cellular actin cytoskeleton through focal adhesions [26]. It is known that the attachment of substrate-dependent cells, such as fibroblasts and osteoblast, to a substratum is a synchronized process, involving cytoskeleton reorganization, cell spreading, and formation of focal contact [27, 28]. The cell adhesion of M1 samples shows (Figs. 2b, 3b) extensive network of filopodium. These actin cytoskeletons were helpful in sensing and exploring the local environment during the cell-biomaterial interaction and useful in maximizing the cell–cell contacts by polymerization of actin filaments. A maximum level of cell–cell contacts was observed in the M2 and M3 sample (Figs. 2c–d, 3c–d), since long and directional lamellipodium were visible, irrespective of the cell lines (Saos-2 and L929). The M2 and M3 glass ceramics exhibit intermediate level of actin filament extension and it helped in

maximizing the cell–cell contacts by extending the 'dendritic' network of actin extension lamellipodium. In M1 sample, the cells are more flattened with low level of actin filament protrusion [28, 29]. It is assumed that the actin cytoskeleton can be regulated by the ions released from the biomaterial that trigger signal transduction event and activate a family of protein that can help reorganization of cytoskeleton [30]. In particular, previous studies using NIH3T3 cells showed that the early spreading events are characterized by the extension of filipodium and cell–cell contacts by lamellipodium [31].

It has been reported that cytocompatlibilty property was improved, when the B_2O_3 and F^- was added in an optimized concentration [31]. It has been observed that optimized concentration of B_2O_3, and F^- improve the osteoblast cell response and also exhibit bactericidal effect [32]. For instance, fluoride-containing HAp supports the cellular functionality. Alternatively, if B_2O_3 and F^- release is significantly higher, it shows the bactericidal effect [33]. The proliferating cell numbers obtained for the fluoridated GC samples (M1, M2 and M3) were greater than control glass cover slip, supporting the fact that fluoride has a stimulatory effect on cellular growth [34, 35].

In the present case, the results from MTT assay demonstrate that maximum numbers of metabolically active cells were present in M1 samples after 2 days of culture and the result clearly reveals that M1 GC was more cytocompatible than the M2 and M3 samples (Fig. 4). MTT results also corroborate with our observation that M1 GC shows better cell flattening/spreading than other two compositions (Figs. 2, 3). It can be further noted that the cytocompatibility behavior of a material varies with cell line [31]. In the present case, it is however found that cellular functionality in terms of cell adhesion is better in M1 than M2 and M3, irrespective of cell line.

4.2 Possible influence of in vitro dissolution on cellular viability

In our earlier study, we reported the in vitro dissolution characteristics of the presently investigated glass ceramics [21]. One of the important results was the formation of CaP-like layer [21]. It should be clear that such biomineralisation ability of the glass ceramic is one of the underlying reasons for exhibiting good cellular adhesion and supporting osteoconduction property of the investigated glass ceramic. As far as the release of different ions concerned, in vitro dissolution results indicate that 0.16 ppm F^- ions are released from M2 glass ceramic over the period of 1 week [21]. Also, our earlier work reported that the dissolution of K^+ and Mg^{2+} ions from M1 glass ceramic is much higher than M2 and M3, which have comparable metal ion leaching rate. For M1 sample, around 225 mg/l of K^+ ions and 4.75 mg/l of Mg^{2+} ions are leached over a period of 8 weeks. In view of the above information as well as considering that our cell culture experiments are conducted for less than a week, it is possible that metal ions/F^- ion are released although to lower extents, from M1, M2 or M3 glass ceramic during our in vitro testing. This is particularly true as leaching of ions from glass ceramic is kinetically driven process and thereby, is time dependent. From the above, it should be clear that lower F^- content and leaching of K^+ or Mg^{2+} ions is from M1 glass ceramic, both contribute to much better cytocompatibility.

Another factor is the difference in B_2O_3, a precursor for boric acid in cell culture media. The boron derivatives seem to be more active than boric acid with respect to the release of proteoglycans and proteins from fibroblasts, whereas boric acid is the most effective compound for release of proteoglycans from skeleton. In a different study, Fu et al. demonstrated that boron based bioactive glass ceramic scaffolds can exhibit significant proliferation of the MLO-A5 as well as on bone marrow stromal cells [36]. An important observation was that a threshold concentration of B_2O_3 is essential for the optimum cell growth and above a minimum threshold of B_2O_3 concentration, the cellular growth was inhibited. Based on our previous results of dissolution study [21] as well as on the basis of the MTT results of the present study, it can be said that M1 and M2 samples have good biocompatibility than those from M3 sample. It is also known that M1 and M2 samples contain 5.17 and 5.25 wt.% B_2O_3, respectively. M3 sample with higher B_2O_3 content of 10.02 wt.% shows minimum number of metabolically active cells (Fig. 4). Therefore, our results are in line with earlier observations that cellular functionality is inhibited at higher B_2O_3 concentration and the minimum threshold, as indicated by Fu et al. [36], should lie in the present case somewhere between 5 and 10 wt.%.

It has been reported in literature that B_2O_3 on material surface or in solution stimulates the activity of intra and extracellular protease, which play a vital role in increasing the ECM and wound healing process [35]. The ALP activity on GC is a phenotypic marker for early-stage differentiated osteoblasts. In M1 sample, the highest percent of viability of metabolically active cell is measured, when compared to other two compositions further corroborate highest ALP activity in the M1 sample. From MTT results of metabolically active cells, it is clear that after 2 days of culture, % viability decreased, due to leaching of F^- ions in culture media, which affects the cytocompatibility. The specific ALP enzyme activity was highest at the later stage of the cell growth. In view of the above observation as well as looking at Table 1, it appears that lower F^- content also favors cell viability and support osteoconduction property.

4.3 Antimicrobial property

In contrast, a different trend is recorded when antimicrobial property was tested against Gram-positive *S. epidermidis* and Gram negative bacteria *E. coli*. It is found that M3 sample exhibits good antimicrobial property against both Gram positive and Gram negative bacteria (See Figs. 6d, 7d). This observation can be attributed to the difference in composition of glass ceramics. From Table 1, it should be clear that M3 contain 2.53% F^- and 42.57% SiO_2; while M2 has 3.85% F^- and 48.94% SiO_2. Despite higher fluorine content, M2 has less quantified antimicrobial property (84% CFU/ml in M3 vs. 77% CFU/ml in M2) than M3. It appears that higher amount of SiO_2 in M2 suppresses beneficial effect of F^- as far as bactericidal effect is concerned.

It is reported that silicon oxide matrix containing any antimicrobial component demonstrates its antimicrobial activity against Gram-positive as well as Gram-negative bacterium. Coppelo and co-workers also observed that presence of 1% of antimicrobial compound in silica matrix reduces 99% colony-forming units (CFU) of Gram-negative bacterium [37]. However, a reduction in CFU/ml takes place for Gram-positive bacterium, when antimicrobial compound content was increased to 1.5%.

Antimicrobial actions of the F^-component in GC were not much different for Gram-positive and Gram-negative bacterial cells. The effect of B_2O_3 and F^- on the Gram-positive and Gram-negative bacterial cells decreases after a certain concentration, because of the difference in the structure of cell wall. The bacterial cell wall is a porous barrier that allows the entry of antimicrobial components and the bacterial cell wall is the ideal target for the action of antimicrobial agents [38, 39]. The peptidoglycan layer is a specific membrane feature of the bacterial cell wall, but the Gram-negative bacterial (*E. coli*) have an additional outer layer, made up of lipopolysaccaride and proteins, which increases the overall negative charge of the outer membrane. A lipopolysaccahride is a negative charge moiety, which enhances the resistance of Gram negative bacteria and prevents penetration of leached antimicrobial ions/components like F^- and B_2O_3. In Fig. 9, it is to be noticed that the mean optical density values of *E. coli* are significantly higher compared to that of *S. epidermidis* (Fig. 8) in all the GC samples. Also, it is reported that the extra-cellular peptidoglycane and protein significantly influences the antimicrobial activity of the sample [40–43]. While the role of F^- ion on difference in antimicrobial property is explained above, the influence of B_2O_3 needs to be mentioned. The presence of higher amount of B_2O_3 in M3, than that in M1 and M2, releases more boric acid and this appears to target more the bacterial cell wall [44, 45]. Overall, the leached ions effectively inhibited the Gram-positive and Gram-negative bacterial growth. The antimicrobial activity is associated with the electrostatic attraction between B_2O_3 and F^- ions and bacterial cell. Also, the concentration of leached ions is importantly associated with the formation of the pits in the cell membrane and changes the membrane permeability. We hypothesized that change in the cell membrane permeability of the Gram-positive and Gram-negative bacterial is responsible for the differences in the antimicrobial property of GC. The implication of this work is important. For as the combination of flexural strength, hardness and Elastic modulus is concerned, M2 has best set of properties, followed by M1 [21] from the present work, it is clear that M1 among the best substrate for enhanced cell viability and osteoblast differentiation. On the other hand, M2 has the good antimicrobial property against both *E. coli* and *S. epidermidis* bacterial strains. Therefore, M2 glass ceramic would be preferred for dental restoration application, while M1 can have potential application in bone replacement, which requires a good combination of cellular functionality and physical property.

5 Conclusions

Based on the experimental results obtained with a series in vitro biochemical assays as well as antimicrobial property evaluation, the following can be concluded:

(a) One of the important results is that boron and fluorine component in the SiO_2–MgO–Al_2O_3–K_2O–B_2O_3–F glass ceramics with fluorophologopite as major crystalline phase have significant influence on cytocompatibility, cell adhesion and cell attachment properties. The glass ceramic with lowest F^- content shows highest cell viability and also supports osteoconduction.

(b) Irrespective of the cell line (L929 and Saos-2), the cell spreading, cytoplasmic extension, are observed on all the investigated glass ceramic qualitatively to similar extent. In particular, the glass ceramic with lowest fluorine content of 1.08% shows maximum cellular viability property as well as cellular adhesion/spreading. The good biocompatibility of glass ceramics with less amount of boron and fluorine content are ascribed to the composition effect and/or microstructure.

(c) (c) The glass ceramics with highest B_2O_3 content (10.02%) and moderate F^- (2.53%) exhibits best antimicrobial property against both Gram negative (*E. coli*) and Gram positive (*S. epidermidis*) bacteria.

Acknowledgements The authors would like to acknowledge the Department of Biotechnology, Government of India for the financial support.

References

1. Kanchanarat N, Bandyopadhyay-Ghosh S, Reaney MI, Brook MI, Hatton VP. Microstructure and mechanical properties of fluorcanasite glass-ceramics for biomedical applications. J Mater Sci. 2008;43:759–65.
2. Gonzalez P, Serra J, Liste S, Chiuss S, Leon B, Perez-Amor M, et al. New biomorphic SiC ceramics coated with bioactive glass for biomedical applications. Biomaterials. 2003;24:4827–32.
3. Verne E, Ferraris S, Miola M, Fucale G, Maina G, Martinasso G, et al. Synthesis and characterisation of bioactive and antibacterial glass-ceramic Part 1—microstructure, properties and biological behaviour. Adv Appl Ceram. 2008;107:234–44.
4. Larry LH. Bioceramics: from concept to clinic. J Am Ceram Soc. 1991;74:1487–510.
5. Chen X, Hench LL, Greenspan D, Zhong J, Zhang X. Investigation on phase separation, nucleation and crystallization in bioactive glass-ceramics containing fluorophlogopite and fluorapatite. Ceram Int. 1998;24:401–10.
6. Nath S, Bodhak S, Basu B. HDPE–Al_2O_3–HAp composites for biomedical applications: processing and characterization. J Biomed Mater Res B Appl Biomater. 2009;88:1–11.
7. Ning J, Yao A, Wang D, Huang W, Fu H, Liu X, et al. Synthesis and in vitro bioactivity of a borate-based bioglass. Mater Lett. 2007;61:5223–6.
8. Liang W, Rahaman NM, Day ED, Marion WN, Riley CG, Mao JJ. Bioactive borate glass scaffold for bone tissue engineering. J Non-Cryst Solids. 2008;354:1690–6.
9. Benderdour M, Van Bui T, Hess K, Dicko A, Belleville F, Dousset B. Effects of boron derivative on extracellular matrix formations. J Trace Elements Med Biol. 2000;14:168–73.
10. Benderdour M, Hess K, Dzondo-Gade M, Nabet P, Belleville F, Dousset B. Modulates extracellular matrix and TNFα synthesis in human fibroblasts. Biochem Biophys Res Commun. 1998;246:346–51.
11. Kim HM. Ceramic bioactivity and related biomimetic strategy. Curr Opinion Solid State Mater Sci. 2003;7:289–99.
12. Harrison J, Melville AJ, Forsythe JS, Muddle BC, Trounson AO, Gross KA, et al. Sintered hydroxyfluorapatites—IV: the effect of fluoride substitutions upon colonisation of hydroxyapatites by mouse embryonic stem cells. Biomaterial. 2004;25:4977–86.
13. Bibby J, Bubb N, Wood DM. Fluorapatite-mullite glass sputter coated Ti6Al4V for biomedical applications. J Mater Sci: Mater Med. 2005;16:379–85.
14. Kumar R, Kalmodia S, Nath S, Sigh D, Basu B. Phase assemblage study and cytocompatibility property of heat treated potassium magnesium phosphate–silicate ceramics. J Mater Sci: Mater Med. 2009;20:1689–95.
15. Xiang Q, Liu Y, Sheng X, Dan X. Preparation of mica-based glass-ceramics with needle-like fluorapatite. Dent Mater. 2007;23:251–8.
16. Alemany MI, Velasquez P, de la Casa-Lillo MA, De Aza PN. Effect of materials' processing methods on the 'in vitro' bioactivity of wollastonite glass-ceramic materials. J Non-Cryst Solids. 2005;351:1716–26.
17. Salman MS, Salama NS, Darwish H, Mosallam Abo HA. HA forming ability of some glass-ceramics of the $CaMgSi_2O_6$–$Ca_5(PO_4)_3F$–$CaAl_2SiO_6$ system. Ceram Int. 2006;32:357–64.
18. Brook IM, Craig GT, Lamb DJ. In vitro interaction between primary bone organ cultures, glass-ionomer cements and hydroxyapatite/tricalcium phosphate ceramics. Biomaterials. 1991;12:179–86.
19. Soljanto P, Rehtijrvi P, Tuovinen HO. Ferrous iron oxidation by *thiobacillus ferrooxidans*: inhibition by finely ground particles. Geomicrobiol J. 1980;2:1–12.
20. Silver FH, Christiansen DL. Biomaterials science and biocompatibility. 1st ed. Springer; 1999. p. 318.
21. Molla RA, Basu B. Microstructure, mechanical, and in vitro properties of mica glass-ceramics with varying fluorine content. J Mater Sci: Mater Med. 2009;20:869–82.
22. Mosmann T. Rapid colorimetric assay for cellular growth and survival: application to proliferation and cytotoxicity assays. J Immunol Methods. 1983;65:55–63.
23. Albert B, Johanson A, Lewis J, Raff M, Roberts K, Walter P. Molecular biology of the cell. 4th ed. God and Science; 2002.
24. Höche T, Habelitz S, Avramov I. Crystal morphology engineering in SiO_2–Al_2O_3–MgO–K_2O–Na_2O–F mica glass-ceramics. Acta Mater. 1999;47:735–44.
25. Zuwei M, Masaya K, Ryuji I, Seeram R. Potential of nanofiber matrix as tissue-engineering scaffolds. Tissue Eng. 2005;11:101–9.
26. Buddy DR, Allan SH, Frederick JS, Jack EL. Biomaterials science: an introduction to materials in medicine. 2nd ed. Elsevier Academic Press; 2004.
27. West KA, Zhang H, Brown MC, et al. The LD4 motif of paxillin regulates cell spreading and motility through an interaction with paxillin kinase linker (PKL). J Cell Biol. 2001;154:161–76.
28. Misra A, Pei Zhi Lim R, Wu Z, Thirumaran T. N-WASP plays a critical role in fibroblast adhesion and spreading. Biochem Biophys Res Commun. 2007;364:908–12.
29. Louise PC. Role of actin-filament disassembly in lamellipodium protrusion in motile cells revealed using the drug jasplakinolide. Curr Biol. 1999;9:1095–105.
30. Pavalko FM, Otey CA. Role of adhesion molecule cytoplasmic domains in mediating interactions with the cytoskeleton. Proc Soc Exp Biol Med. 1994;205:282–93.
31. Issa Y, Brunton P, Waters CM, Watts DC. Cytotoxicity of metal ions to human oligodendroglial cells and human gingival fibroblasts assessed by mitochondrial dehydrogenase activity. Dent Mater. 2008;24:281–7.
32. Benderdour M, Hess K, Dzondo-Gadet M, Dousset B, Nabet P, Belleville E. Effect of boric acid solution on cartilage metabolism. Biochem Biophys Res Comm. 1997;234:263–8.
33. Farley JR, Wergedal JE, Baylink DJ. Fluoride directly stimulates proliferation and alkaline phosphatase activity of bone-forming cells. Science. 1983;22:330–2.
34. Campoccia D, Arciola CR, Cervellati M, Maltarello MC, Montanaro L. In vitro behaviour of bone marrow-derived mesenchymal cells cultured on fluorhydroxyapatite-coated substrata with different roughness. Biomaterials. 2003;24:587–96.
35. Dure-Smith BA, Kraenzlin ME, Farley SM, Libanati CR, Schulz EE, Baylink DJ. Fluoride therapy for osteoporosis: a review of dose response, duration of treatment, and skeletal sites of action. Calcif Tissue Int. 1991;49:64–7.
36. Fu Hailuo, et al. In vitro evaluation of borate-based bioactive glass scaffolds prepared by a polymer foam replication method. Mater Sci Eng C. 2009;29:2275–81.
37. Copello GJ, Teves S, Degrossi J, D'Aquino M, Desimone MF, Diaz LE. Antimicrobial activity on glass materials subject to disinfectant xerogel coating. J Ind Microbiol Biotechnol. 2006;33:343–8.
38. Yuehuei HA, Richard JF. Concise review of mechanisms of bacterial adhesion to biomaterial surfaces. J Biomed Mater Res B Appl Biomater. 1998;43:338–48.
39. Michal JPJR, Chan ECS, Noel RK. Microbiology. 5th ed. Tata McGraw-Hill; 1993.

40. Jun Sung KDVM, Eunye Kuk KNY, Jong-Ho K, Sung Jin P, Hu Jang LDVM, So Hyun KDVM, et al. Antimicrobial effects of silver nanoparticles. Nanomedicine. 2007;3:95–101.
41. Vitale-Brovarone C, Miola M, Balagna C, Vern E. 3D-glass–ceramic scaffolds with antibacterial properties for bone grafting. Chem Eng J. 2008;137:129–36.
42. Ivan S, Branka SS. Silver nanoparticles as antimicrobial agent: a case study on *E. coli* as a model for Gram-negative bacteria. J Colloid Interf Sci. 2004;275:177–82.
43. Niall S, Brendan D, Declan E, McCormack, John C, Martha H, et al. Prevention of *Staphylococcus epidermidis* biofilm formation using a low-temperature processed silver-doped phenyltrieth-oxysilane sol–gel coating. Biomaterials. 2008;29:963–9.
44. Houlsby RD, Ghajar M, Chavez GO. Antimicrobial activity of borate-buffered solutions. J Antimicrob Agents Chemother. 1986; 29:803–6.
45. Watanabe S, Fujita T, Sakamoto M. Antimicrobial properties of boric acid esters of alcohols. J Am Oil Chem Soc. 1988;65:1479–82.